MULTI-SCALE REPRESENTATION OF DEFORMATIONS VIA WAVELET TRANSFORM ON BELTRAMI COEFFICIENTS

TSZ CHING NG, KA CHUN LAM AND LOK MING LUI

Abstract. Analyzing the deformation pattern of an object is crucial in various fields, such as in computer visions and medical imaging. A deformation can be considered as a combination of local and global deformations at different locations. To fully understand the deformation pattern, extracting the deformation of various scales and locations is necessary. We propose an algorithm for the multi-scale decomposition of a deformation using quasi-conformal theories. A deformation of an object can be described as a diffeomorphism. The diffeomorphism can then be represented by its associated Beltrami coefficient (BC), which measures the local geometric (conformality) distortion of the deformation. The BC is a complex-valued function defined on the source domain. By applying the wavelet transform on the BC, the BC can be decomposed into different components of different frequencies compactly supported in different sub-domains. Quasi-conformal maps associated to different components of the BC can be reconstructed by solving the Beltrami's equation. A multi-scale decomposition of the deformation can then be constructed. We test the proposed algorithm on synthetic examples as well as real medical data. Experimental results show the efficacy of our proposed model to decompose a deformation at multiple scales and locations.

Key words. Deformation, multi-scale decomposition, wavelet transform, Beltrami coefficient, quasi-conformal map, conformality distortion

1. Introduction. Analyzing the deformation pattern of an object has central importance in various fields, such as in computer visions and medical shape analysis [25, 2]. For example, in medical imaging, finding abnormal deformation pattern of the cardiac motion is crucial for understanding heart disease [31, 3, 23]. While in computer visions, the analysis of deformation pattern is necessary for video tracking [32]. Developing an effective mathematical model to analyze deformations is therefore of great research interest.

A deformation is often described as a diffeomorphism of the domain in which the object is embedded. A deformation can be regarded as a combination of local and global deformations at different scales and locations. In order to understand the deformation pattern thoroughly, the extraction of deformations at different scales and locations is essential. To achieve this goal, an algorithm to decompose a diffeomorphism into different components of different scales is needed. A major challenge is that each components of the decomposition must remain diffeomorphic, as they describe deformations at multiple scales. Simply applying the multi-scale decomposition on the coordinate functions of the diffeomorphism does not work, since the diffeomorphic property of each components can be severely lost. A better representation of a diffeomorphism, with which multi-scale diffeomorphic decomposition can be easily achieved, must be used.

In this paper, we propose a novel algorithm for the multi-scale decomposition of a deformation via quasi-conformal theories. Given a deformation represented by a diffeomorphism, the associated complex-valued function, called the *Beltrami coefficient (BC)*, is computed. The BC measures the conformality or local geometric distortion of the diffeomorphism, which has supreme norm strictly less than 1. Given a diffeomorphism, its BC can be easily computed from the Beltrami's equation. Conversely, given a BC, the associated quasi-conformal map can be reconstructed through solving elliptic PDEs derived from the Beltrami's equation. Unlike the coordinate functions, the BC has much less constraints to ensure the associated map is diffeomorphic. The only constraint is that its supreme norm is strictly less than 1, which can be easily enforced.

In recent years, BCs have been applied to represent diffeomorphisms for image/surface registration[19, 6, 16], video compression[18] and texture map compression[18]. In this work, our main goal is to apply the BC to construct the multi-scale decomposition of a deformation. The extracted local and global deformations at different locations can be utilized for shape analysis. More precisely, by applying the wavelet transform on the BC, the BC can be decomposed into different components of different frequencies compactly supported in different sub-domains. Quasi-conformal maps associated to different components of various scales can be reconstructed, which give the multi-scale diffeomorphic decomposition of the deformation. With the decomposition, a thorough multi-scale analysis of the deformation can be carried out. We have tested the proposed algorithm on synthetic examples as well as real medical images. Experimental results demonstrate the effectiveness of the proposed model to decompose a deformation into diffeomorphic components at multiple scales.

To summarize, the main contribution of this paper is to explore the efficacy of a wavelet-based algorithm for the multi-scale decomposition of a deformation. We propose to apply the wavelet transform on the BC, with which the multi-scale components of the deformation can be defined. The rest of the paper is organized as follows. In Section 2, some previous works closely related to this paper are presented. Some basic mathematical theories necessary for this work are described in Section 3. Our proposed algorithm for multi-scale deformation extraction is explained in details in Section 4. Experimental results are reported in Section 5. The paper is concluded and some future works are discussed in Section 6.

2. Previous work. We briefly review some previous works closely related to this paper.

In this work, registration is required to extract deformations. Registration aims to establish meaningful one-to-one correspondences between different subjects [13, 34]. With the registration result, the deformation field can be obtained for further analysis. In this work, a deformation field is described as a diffeomorphism between corresponding data. Different registration algorithms have been proposed for obtaining the deformation fields. Basically, registration models can be classified into two categories [25], namely, the landmark-based model and the intensity-based model. Landmark-based models aim to guide registration using characteristic features, which can be uniquely identified across different data. For example, the *Thin-Plate Spline (TPS)* registration model proposed by Bookstein et al. [4] aligns landmarks via the biharmonic regularizer. Using the framework of quasi-conformal theories, several works have been proposed to tackle the landmark-based registration problem [16, 6]. Intensity-based registration models aim to guide the registration process by matching the intensity information. A number of intensity-based registration algorithms have been developed recently. To list a few, the Diffeomorphic Demons registration method has been proposed in [29], which extended Thirion's demons algorithm [27]. The algorithm obtained the registration result in the space of diffeomorphic transformations. Glocker et al. [10, 9] proposed the DROP algorithm to register images using the Markov random field formulation.

With the deformation fields, different techniques can be applied to analyze the hidden information from the registration results. For instance, the Support Vector Machines (SVM) has been proposed for studying statistical differences between anatomical shapes [11]. Analysis of deformation fields using Wavelet SVM (WSVM) has also been proposed in [21]. Another commonly used approach is to construct descriptors for statistical models to perform comparison between different data [12, 33].

To name a few, Røgen and Bohr [22] proposed a family of global protein shape descriptors for the classification of different proteins by their structures. In [15], a 3D Zernike descriptor has been proposed for the shape analysis of protein with surface representation. Detection of shape deformities from the deformation field using quasi-conformal theories has also been proposed. Lui et. al [20] proposed to use Beltrami coefficients to locate abnormal non-rigid changes over time. A quasi-conformal metric for deformation classification has also been introduced by Taimouri and Hua [26] to classify the left ventricle deformations of myopathic and control subjects.

To analyze a deformation with different geometric scales or directions, various algorithms for the decomposition of vector fields have been proposed. Tong et al. [28] proposed a variational multi-scale decomposition of vector fields. The vector fields were decomposed into the divergent-free part, the cur-free part and the harmonic part using the idea of Heltmotz-Hodge decomposition. Abeyratne [1] applied the Cauchy-Navier equation to describe the elastic deformation and a wavelet-based approach was proposed for the multi-scale deformation analysis of objects with spherical boundary. Kaplan and Donoho [14] proposed the Morphlet Transform to obtain a multi-scale representation for diffeomorphisms. Under the Morphlet framework, the representation is equipped with a forward transform with coefficients, which are organized dyadically. Its inverse transform was also guaranteed to generate diffeomorphism under certain sampling conditions. Sommer et al. [24] proposed a multi-scale kernel bundle to represent large deformations in medical imaging. As the registration results obtained from the *LDDMM* framework are greatly affected by the choice of the kernel, this work extends the *LDDMM* framework by allowing multiple kernels at different scales for controlling the registration. In [5], Chen et al. proposed an efficient method to compute the Morse decomposition of vector fields to extract and visualize the vector field topology. In this work, our goal is to extract diffeomorphic components of a deformation in different scales and locations. Both the local and global deformation patterns are extracted through applying a wavelet transform on the Beltrami representation of a diffeomorphism. The Beltrami representation has been applied in [18] for texture map and video compression. It has also been applied for image and surface registration [6, 16].

3. Mathematical Background. In this section, we describe some basic mathematical theories relevant to this work. For details, we refer readers to [8, 7, 17].

A surface S with a conformal structure is called a *Riemann surface*. Given two Riemann surfaces M and N, a map $f : M \to N$ is *conformal* if it preserves the surface metric up to a multiplicative factor called the *conformal factor*. An immediate consequence is that every conformal map preserves angles. With the angle-preserving property, a conformal map effectively preserves the local geometry of the surface structure.

A generalization of conformal maps is the *quasi-conformal* maps, which are orientation preserving homeomorphisms between Riemann surfaces with bounded conformality distortion, in the sense that their first order approximations take small circles to small ellipses of bounded eccentricity [8]. Mathematically, $f\colon \mathbb{C} \to \mathbb{C}$ is quasi-conformal provided that it satisfies the Beltrami equation:

$$\frac{\partial f}{\partial \overline{z}} = \mu(z)\frac{\partial f}{\partial z}. \tag{3.1}$$

for some complex-valued function μ satisfying $||\mu||_\infty < 1$. μ is called the *Beltrami coefficient*, which is a measure of non-conformality. It measures how far the map at each point is deviated from a conformal map. In particular, the map f is conformal around a small neighborhood of p when $\mu(p) = 0$. Infinitesimally, around a point p, f may be expressed with respect to its local parameter as follows:

$$\begin{aligned} f(z) &\approx f(p) + f_z(p)z + f_{\overline{z}}(p)\overline{z} \\ &= f(p) + f_z(p)(z + \mu(p)\overline{z}). \end{aligned} \tag{3.2}$$

Obviously, f is not conformal if and only if $\mu(p) \neq 0$. Inside the local parameter domain, f may be considered as a map composes of a translation to $f(p)$ together with a stretch map $S(z) = z + \mu(p)\overline{z}$, which is post-composed by a multiplication of $f_z(p)$, which is conformal. All the conformal distortion of $S(z)$ is caused by $\mu(p)$. $S(z)$ is the map that causes f to map a small circle to a small ellipse. From $\mu(p)$, we can determine the angles of the directions of maximal magnification and shrinking of $S(z)$ and the amount of them as well. Specifically, the angle of maximal magnification is $\arg(\mu(p))/2$ with magnifying factor $1 + |\mu(p)|$; The angle of maximal shrinking is the orthogonal angle $(\arg(\mu(p)) - \pi)/2$ with shrinking factor $1 - |\mu(p)|$. Thus, the Beltrami coefficient μ gives us lots of information about the properties of the map.

The maximal dilation of f is given by:

$$K(f) = \frac{1 + ||\mu||_\infty}{1 - ||\mu||_\infty}. \tag{3.3}$$

Given a Beltrami coefficient $\mu : \mathbb{C} \to \mathbb{C}$ with $\|\mu\|_\infty < 1$. There is always a quasiconformal mapping from $\mathbb{C}$ onto itself which satisfies the Beltrami's equation in the distribution sense [8].

4. Multi-scale extraction of deformation. In this section, we explain our algorithm for the multi-scale decomposition of a deformation in details.

4.1. Deformations as diffeomorphisms. In this work, we formulate a deformation as a diffeomorphism of the domain in which the object is embedded. Suppose an object is embedded in a 2D domain $D \subset \mathbb{R}^2$. A deformation can be formulated as a diffeomorphism $f : D \to D$.

An object is often captured as an image. Suppose the image of the object at the initial ($t = 0$) and final ($t = 1$) time are denoted by $I_1 : D \to \mathbb{R}$ and $I_2 : D \to \mathbb{R}$ respectively. We can find the deformation by computing the diffeomorphic registration between two images.

We apply the quasi-conformal registration algorithm to obtain the diffeomorphic registration. The basic idea is to find a pair of functions $\nu : D \to \mathbb{C}$ and $f : D \to D$, which minimizes:

$$E_{QCR}(\nu, f) = \int_D |\nu|^2 + |\nabla\nu|^2 + \alpha(I_1 - I_2(f))^2 \tag{4.1}$$

subject to the constraints that:

- ν is the BC of f;
- $||\nu||_\infty < 1$ and/or
- $f(p_i) = q_i$ for $i = 1, 2, ..., n$.

Here, $\{p_i\}_{i=1}^n$ and $\{q_i\}_{i=1}^n$ are corresponding landmark points or curves of the two images respectively. In the case that landmark features can be accurately delineated, enforcing the landmark constraint (the third constraint) can lead to a more accurate diffeomorphic quasi-conformal registration. For details of the quasi-conformal registration, we refer the readers to [16].

Once the diffeomorphic registration is obtained, the processing on the diffeomorphism can be carried out to decompose the deformation into components at multiple scales and locations.

4.2. Beltrami coefficient and diffeomorphisms. The multi-scale decomposition of a deformation can be extracted by performing a multiscale decomposition, such as the wavelet transform, on the diffeomorphism. A basic requirement is that each components of the decomposition must be diffeomorphic, as they represent diffeomorphic deformation at different scales and different locations.

A diffeomorphism $f : D \to D$ is often represented by its coordinate functions $f(x, y) = (U(x, y), V(x, y))$. Applying the multiscale decomposition on U and V directly inevitably leads to a severe loss of bijectivity (see Figure 5.6). A remedy is to develop a decomposition algorithm while ensuring the Jacobians of each components are positive. However, it is a rather challenging problem.

To effectively decompose a deformation into diffeomorphic components, we apply the Beltrami coefficient to represent a diffeomorphism. Given a diffeomorphism $f : D \to D$, according to the Beltrami's equation, it is associated with a unique complex-valued function $\mu(f) : D \to \mathbb{C}$ defined by:

$$\mu(f)(z) = \left(\frac{\partial f}{\partial \bar{z}}\right) / \left(\frac{\partial f}{\partial z}\right). \tag{4.2}$$

As f is diffeomorphic, $||\mu(f)||_\infty < 1$. Conversely, given an admissible Beltrami coefficient $\nu : D \to \mathbb{C}$ with $||\nu||_\infty < 1$, its associated quasi-conformal map can be computed by solving the Beltrami's equation. Suppose $\nu = \rho + i\tau$ and $f^\nu = u + iv$. Let $\alpha = \frac{(\rho-1)^2+\tau^2}{1-\rho^2-\tau^2}$; $\beta = -\frac{2\tau}{1-\rho^2-\tau^2}$; $\gamma = \frac{1+2\rho+\rho^2+\tau^2}{1-\rho^2-\tau^2}$. The Beltrami's equation can be reduced to the following elliptic PDEs:

$$\nabla \cdot \left(A \begin{pmatrix} u_x \\ u_y \end{pmatrix}\right) = 0 \quad \text{and} \quad \nabla \cdot \left(A \begin{pmatrix} v_x \\ v_y \end{pmatrix}\right) = 0 \tag{4.3}$$

where $A = \begin{pmatrix} \alpha & \beta \\ \beta & \gamma \end{pmatrix}$.

In the discrete case, the elliptic PDEs (4.3) can be discretized into sparse positive definite linear systems and can be solved efficiently using the conjugate gradient method. For details, please refer to [18].

The Beltrami coefficient is a desirable representation of a diffeomorphism, since it has the simplest constraint to ensure the bijectivity. To ensure the bijectivity of a mapping f^ν, its Jacobian must be greater than 0 everywhere. The Jacobian of f^ν is closely related to its Beltrami coefficient ν:

$$J(f) = |\frac{\partial f^\nu}{\partial z}|^2(1 - |\nu|^2). \tag{4.4}$$

Hence, if $|\nu| < 1$ everywhere, $J(f)$ is positive everywhere. If D is simply-connected, f^ν can be shown to be diffeomorphic. Therefore, the only constraint on ν to ensure f^ν is diffeomorphic is $||\nu||_\infty < 1$. This can be easily enforced.

4.3. Wavelet transform on Beltrami Coefficient. In this work, our goal is to decompose a deformation into diffeomorphic components at different scales and locations. Thus, we apply the wavelet transform for the spectral decomposition of the BC, which takes spatial and frequency information into consideration. The wavelet expansion allows a more accurate local description and separation of signal characteristics.

We first give a brief introduction on wavelet transformation. For details, we refer the readers to [30].

A *wavelet* ψ is a wave-like compactly supported function, which is generated by another compactly supported function, called the *scaling function* φ. In 1D, the scaling function φ assumes the following property:

$$\varphi(x) = \sum_{k\in\mathbb{Z}} h(k)2^{1/2}\varphi(2x-k), \tag{4.5}$$

where $\{h(k)\}_{k\in\mathbb{Z}}$ is an l^2 sequence of coefficients and is called the *scaling filter*. The wavelet filter $g(k)$ is defined by

$$g(k) = (-1)^k\overline{h(1-k)} \tag{4.6}$$

and the wavelet $\psi(x)$ associated to φ is defined by

$$\psi(x) = \sum_{k\in\mathbb{Z}} g(k)2^{1/2}\varphi(2x-k). \tag{4.7}$$

Then, $\{\psi_{j,k}(x) := 2^{j/2}\varphi(2^jx-k)\}_{j,k\in\mathbb{Z}}$ forms a *wavelet set*.

In 2D, the wavelet orthonormal set generated by the dilations and translations of basic wavelets can also be constructed. The construction is based on a single two-dimensional scaling function $\Phi(x,y)$ and a set of three two-dimensional functions $\Psi^{(1)}(x,y)$, $\Psi^{(2)}(x,y)$ and $\Psi^{(3)}(x,y)$. Let $\varphi(x)$ and $\psi(x)$ be the scaling and wavelet functions. The 2D scaling and wavelet functions are defined as follows:

$$\begin{aligned}&\Phi(x,y) = \varphi(x)\varphi(y);\ \Psi^{(1)}(x,y) = \varphi(x)\psi(y);\\ &\Psi^{(2)}(x,y) = \psi(x)\varphi(y);\ \Psi^{(3)}(x,y) = \psi(x)\psi(y).\end{aligned} \tag{4.8}$$

Then, the collection $\{\Psi^{(i)}_{j,k_1,k_2}(x,y) := 2^j\Psi^{(i)}(2^jx-k_1, 2^jy-k_2)\}_{1\leq i\leq 3, j,k_1,k_2\in\mathbb{Z}}$ forms an orthonormal set of functions. In particular, for every $f(x,y)\in C^0_c$,

$$f(x,y) = \sum_{i=1}^{3}\sum_{l\in\mathbb{Z}}\sum_{k_1\in\mathbb{Z}}\sum_{k_2\in\mathbb{Z}} < f, \Psi^{(i)}_{l,k_1,k_2} > \Psi^{(i)}_{l,k_1,k_2}(x,y), \tag{4.9}$$

where $< g_1, g_2 > := \int g_1\overline{g_2}$. The above wavelet expansion decomposes a function into components at different locations with different frequencies. The wavelet expansion represents a function in both the spatial and frequency domains at the same time. Thus, it overcomes a major problem of Fourier expansion that it has only frequency resolution but no spatial resolution.

To obtain a multi-scale representation (MSR) of a deformation, we propose to apply the wavelet decomposition on the Beltrami coefficient associated to the deformation. As discussed earlier, every deformation can be described as a diffeomorphism $f: D_1\to D_2$. The Beltrami coefficient $\mu(f)$ of f, which measures the local geometric distortion, can be easily computed from the Beltrami's equation. By applying the wavelet expansion on $\mu(f)$, the multi-scale decomposition of the deformation can be obtained. It is described in the following definition.

Definition 4.1. *Let $f : \mathbb{C} \to \mathbb{C}$ be a diffeomorphism representing a deformation. Let $\mu(f) : \mathbb{C} \to \mathbb{C}$ be the Beltrami coefficient of f. Suppose:*

$$\mu(f)(x,y) = \sum_{i=1}^{3} \sum_{l\in\mathbb{Z}} \sum_{k_1\in\mathbb{Z}} \sum_{k_2\in\mathbb{Z}} \hat{\mu}(i,l,k_1,k_2)\Psi^{(i)}_{l,k_1,k_2}(x,y), \tag{4.10}$$

where $\hat{\mu}(i,l,k_1,k_2) =< \mu(f), \Psi^{(i)}_{l,k_1,k_2} >$.

1. *The collection of coefficients $\{\hat{\mu}(i,l,k_1,k_2)\}_{1\leq i\leq 3, j, k_1,k_2\in\mathbb{Z}}$ are called the (wavelet) decomposition coefficients of the deformation f.*
2. *Let $U_j := \mathcal{T}(\mathbf{Span}(\{\Psi^{(i)}(j,k_1,k_2)\}_{1\leq i\leq 3, k_1,k_2\in\mathbb{Z}}))$, where $\mathcal{T}$ is the truncation operator to enforce the supreme norm of a complex-valued function to be strictly less than 1. U_j is called the set of deformation distortions at scale j. Define: $V_j := \mathbf{LBS}(U_j)$, where* **LBS** *converts a Beltrami coefficient to its associated quasi-conformal map according to equation 4.3, with the normalization that the map fixes 0, 1 and ∞. V_j is called the set of deformations at scale j.*
3. *Let:*

$$\mathcal{P}_j(\mu(f)) := \mathcal{T}\left(\sum_{i=1}^{3} \sum_{k_1\in\mathbb{Z}} \sum_{k_2\in\mathbb{Z}} \hat{\mu}(i,j,k_1,k_2)\Psi^{(i)}_{j,k_1,k_2}(x,y)\right) \tag{4.11}$$

   $\mathcal{P}_j$ is called the projection of $\mu(f)$ to the distortion component at scale j. $\mathcal{P}_j(\mu(f))$ is called the distortion component at scale j.
4. *Let $f_j := \mathbf{LBS}(\mathcal{P}_j(\mu(f))) : \mathbb{C} \to \mathbb{C}$. $f_j \in V_j$ is called the deformation component at scale j.*
   The sequence $\{f_j : \mathbb{C} \to \mathbb{C}\}_{j\in\mathbb{Z}}$ is called the multiscale representation (MSR) of the deformation f.
5. *Let Ω be a sub-domain in $\mathbb{C}$. Define the index set $I(j,\Omega)$ by:*

$$I(j,\Omega) := \{(i,k_1,k_2) : 1 \leq i \leq 3, k_1,k_2 \in \mathbb{Z}, \mathbf{supp}(\Psi^{(i)}(j,k_1,k_2)) \subseteq \Omega\}. \tag{4.12}$$

   where $\mathbf{supp}(\Psi^{(i)}(j,k_1,k_2))$ is the support of $\Psi^{(i)}(j,k_1,k_2)$.
   Let:

$$\widetilde{\mu}(\Omega,j) := \mathcal{T}\left(\sum_{(i,k_1,k_2)\in I(j,\Omega)} \hat{\mu}(i,j,k_1,k_2)\Psi^{(i)}_{j,k_1,k_2}(x,y)\right) \tag{4.13}$$

   $\widetilde{\mu}(\Omega,j)$ is called the local deformation distortion at the region Ω and scale j. Consequently, $f_j^{\Omega} := \mathbf{LBS}(\widetilde{\mu}(\Omega,j))$ is called the deformation component of f at the region Ω and scale j.

Remark: Below are some remarks for the above definitions.

1. The sets of deformation distortions at different scales satisfy the following property:

$$U_j \subseteq U_{j+1} \text{ for all } j \in \mathbb{Z}. \tag{4.14}$$

   Each set U_j consists of a collection of Beltrami coefficients of a given frequency related to the scale j.

Similarly, the sets of deformations at different scales satisfies: $V_j \subseteq V_{j+1}$ for all $j \in \mathbb{Z}$. Each set V_j consists of a collection of quasi-conformal maps associated to the Beltrami coefficients in U_j. Thus, the idea of multi-scale decomposition of a deformation can be considered as projecting the deformation into the various sets V_j ($j \in \mathbb{Z}$).

2. Note that the distortion component at a scale j is a complex-valued function, whose supreme norm may not be strictly less than 1. In order to obtain the multi-scale components of a deformation, each distortion component must be a Beltrami coefficient with supreme norm strictly less than 1. This ensures the diffeomorphic property of the associated quasi-conformal map. The truncation operator is to truncate a complex-valued function so that its supreme norm is strictly less than 1. There are several choices of $\mathcal{T}$. A simple choice is to define $\mathcal{T}$ by:

$$\mathcal{T}(\mu) = \mathbf{T}(|\mu|)\frac{\mu}{|\mu|} \tag{4.15}$$

where $\mathbf{T} : [0, +\infty) \to [0, 1)$ is a monotonically increasing function such that $\mathbf{T}(x) = x$ for $x \in [0, 1 - \epsilon]$ and $\lim_{x \to +\infty} \mathbf{T}(x) = 1$. Another choice can be done as follows. Given $\mu : \mathbb{C} \to \mathbb{C}$, we define $\widetilde{\mu} : \mathbb{C} \to \mathbb{C}$ by:

$$\widetilde{\mu}(p) = \min\{|\mu(p)|, 1 - \epsilon\}\frac{\mu(p)}{|\mu(p)|} \text{ for } p \in \mathbb{C}. \tag{4.16}$$

Then, $\mathcal{T}(\mu)$ can be defined as

$$\mathcal{T}(\mu) = \mathbf{argmin}_{\nu:\mathbb{C}\to\mathbb{C}}\{\alpha \int_{\mathbb{C}} |\nabla \nu|^2 + \int_{\mathbb{C}} |\nu - \widetilde{\mu}|^2\}. \tag{4.17}$$

In practice, when the deformation is not extremely large, the supreme norm of its Beltrami coefficient is far below 1. In this case, the distortion component at each scale j usually satisfies the property that its supreme norm is strictly less than 1. Thus, the truncation operator can be omitted in our model.

3. In the above definition, f is a complex-valued function defined on the whole complex plane $\mathbb{C}$. In practice, a deformation f may be defined on a compact simply-connected domain Ω_1 in $\mathbb{C}$. The above definition still applies to this case. For example, suppose Ω_1 is a unit square. For every distortion component $\mathcal{P}_j(\mu(f))$ at scale j ($j \in \mathbb{Z}$), it is associated to a quasi-conformal map $f_j : \Omega_1 \to \Omega_2(\mathcal{P}_j(\mu(f)))$. The target domain $\Omega_2(\mathcal{P}_j(\mu(f)))$ depends on $\mathcal{P}_j(\mu(f))$. We can impose the geometry of the target domain to be a 2D rectangle whose base length is equal to 1. Then, the height of $\Omega_2(\mathcal{P}_j(\mu(f)))$ can be determined by:

$$h = \int_{\Omega_1} \alpha_j u_x^2 + 2\beta_j u_x u_y + \gamma_j u_y^2. \tag{4.18}$$

where u is the real part of the f_j. $\alpha_j = \frac{(\rho_j-1)^2+\tau_j^2}{1-\rho_j^2-\tau_j^2}$; $\beta_j = -\frac{2\tau_j}{1-\rho_j^2-\tau_j^2}$; $\gamma_j = \frac{1+2\rho_j+\rho_j^2+\tau_j^2}{1-\rho_j^2-\tau_j^2}$ with $\mathcal{P}_j(\mu(f)) = \rho_j + i\tau_j$.

4. The local deformation distortion $\widetilde{\mu}(\Omega, j)$ provides information about the local distortion of a certain scale j at a particular location Ω. Note that although $\widetilde{\mu}(\Omega, j)$ is compactly supported in Ω, it has a global effect on the associated

quasi-conformal map. For a large $\widetilde{\mu}(\Omega, j)$, the reconstructed quasi-conformal map may induce deformation outside Ω without conformality distortion (that is, $\widetilde{\mu}(\Omega, j)|_{\Omega^c} = 0$). To ensure that there is no deformation outside Ω, a landmark constrained reconstruction $\mathbf{LBS}_{LM}$ of the quasi-conformal map from the Beltrami coefficient can be applied. The idea of $\mathbf{LBS}_{LM}$ is to solve equation (4.3) subject to the constraint that $f_j^{\Omega} := \mathbf{I}$ outside Ω. In practice, if $|\mu(f)|$ is not very close to 1, the global effect of a Beltrami coefficient compactly supported in a small region is very tiny. Hence, this procedure can be omitted.

The proposed multi-scale representation of a deformation satisfies the following properties.

THEOREM 4.1. *With the same setup as in Definition 4.1,* $\bigcap_{j\in\mathbb{Z}} V_j = \{\mathbf{I} : \mathbb{C} \to \mathbb{C}\}$, *where* $\mathbf{I}$ *is the identity map of* $\mathbb{C}$.

Proof. Our construction forms a multiresolution analysis on $\mathbb{R}^2$, giving a sequence of subspaces $\{U_j\}_{j\in\mathbb{Z}}$ of functions L^2 on $\mathbb{R}^2$. It has the property that $\bigcap_{j\in\mathbb{Z}} U_j = \{\mathbf{0}\}$. Under the normalization that 0, 1 and ∞ are fixed, the quasi-conformal map $f : \mathbb{C} \to \mathbb{C}$ associated to the Beltrami coefficient $\mu \equiv 0$ is the identity map $\mathbf{I}$. Thus, $\bigcap_{j\in\mathbb{Z}} V_j = \{\mathbf{I} : \mathbb{C} \to \mathbb{C}\}$. □

THEOREM 4.2. *Consider a diffeomorphism* $f : \mathbb{C} \to \mathbb{C}$ *that is conformal outside a compact domain* $\Omega \subset \mathbb{C}$. *Given an accuracy* $\epsilon > 0$, *there exist a deformation* f^J *at certain scale* J *whose distortion resemble to the distortion of* f *up to the prescribed accuracy. In other words, for all* $\epsilon > 0$, *there is a* $J \in \mathbb{Z}$ *and a diffeomorphism* $f^J \in V_J$ *such that* $||\mu(f^J) - \mu(f)||_2 < \epsilon$. *Also,* $\lim_{j\to\infty} ||\mu(f) - \mathcal{P}_j(\mu(f))||_2 = 0$.

Proof. Since our construction gives a multiresolution analysis, it has the property that $\nu \in \overline{span}\{U_j\}_{j\in\mathbb{Z}}$ if $\nu \in C_c^0$. As f is conformal outside a compact domain Ω, $\mu(f)(z) = 0$ for all $z \in \mathbb{C} \setminus \Omega$. This implies $\mu(f) \in C_c^0$. Thus, for all $\epsilon > 0$, there is a $J \in \mathbb{Z}$ and a Beltrami coefficient $\tilde{\mu} \in U_J$ such that $||\tilde{\mu} - \mu(f)||_2 \leq \epsilon$. Set $f^J = \mathbf{LBS}(\tilde{\mu})$. Then, $||\mu(f^J) - \mu(f)||_2 < \epsilon$.

Furthermore, given $\epsilon > 0$, there is a $J \in \mathbb{Z}$ and a function $\nu \in U_J$ such that $||\mu(f) - \nu||_2 < \epsilon/2$. For all $j \in \mathbb{Z}$, $U_j \subseteq U_{j+1}$. Hence, $\nu \in U_j$ and $\mathcal{P}_j(\nu) = \nu$ for all $j \geq J$. This implies:

$$
\begin{aligned}
||\mu(f) - \mathcal{P}_j(\mu(f))||_2 &= ||\mu(f) - \nu + \mathcal{P}_j(\nu) - \mathcal{P}_j(\mu(f))||_2 \\
&\leq ||\mu(f) - \nu||_2 + ||\mathcal{P}_j(\mu(f) - \nu)||_2 \\
&\leq 2||\mu(f) - \nu||_2 < \epsilon
\end{aligned}
$$

for all $j \geq J$, where $||\mathcal{P}_j(\mu(f)-\nu)||_2 \leq ||\mu(f)-\nu||_2$ follows from the Bessel's inequality. □

THEOREM 4.3. *Suppose* $f : \mathbb{C} \to \mathbb{C}$ *is a diffeomorphism that is conformal outside a compact domain* $\Omega \subset \mathbb{C}$. . *Suppose* $\mathcal{P}_j$ *is the projection operator of the Beltrami coefficient* $\mu(f)$ *of* f *to the distortion component at scale* j. *Let* f_j *be the deformation component at scale* j. *Then,* f_j *converges locally uniformly to the original deformation* f.

Proof. The proof follows from the Bers-Bojarski theorem, which can be stated as follows: if $\{g_n\}_{n=1}^{\infty}$ is a sequence of K-quasiconformal maps converging locally uniformly to a K-quasiconformal map g and if their associated Beltrami coefficients

$\{\mu_n\}_{n=1}^{\infty}$ converge to μ almost everywhere, then μ is the Beltrami coefficient of g almost everywhere. Now, f_j is the deformation component at scale j. By the compactness of the family of normalized K-quasiconformal maps, we can find a subsequence of $\{f_n\}_{n=1}^{\infty}$, which converges locally uniformly to a K-quasiconformal map. According to Theorem 4.2, $\lim_{j\to\infty} ||\mu(f) - \mathcal{P}_j(\mu(f))||_2 = 0$. Thus, we can find another subsequence, whose Beltrami coefficients converges to μ almost everywhere. By the Bers-Bojarski theorem, any such subsequence converges locally uniformly to the same limit f with Beltrami coefficient μ. We now show that the original sequence must converge locally uniformly to a normalized quasi-conformal map f whose Beltrami coefficient is equal to μ. Suppose not. There exists a neighborhood U and an $\epsilon > 0$ such that for every $k \in \mathbb{N}$, there is a $n_k \geq k$ such that $||f_{n_k}|_U - f|_U||_\infty \geq \epsilon$. Therefore, we get a subsequence $\{f_{n_k}\}_{k=1}^{\infty}$ such that $||f_{n_k}|_U - f|_U||_\infty \geq \epsilon$. Again, by compactness, $\{f_{n_k}\}_{k=1}^{\infty}$ has a locally uniform convergent subsequence $\{f_{n_{k_m}}\}_{m=1}^{\infty}$. However, since $\{f_{n_k}\}_{k=1}^{\infty}$ such that $||f_{n_k}|_U - f|_U||_\infty \geq \epsilon$, $\{f_{n_{k_m}}\}_{m=1}^{\infty}$ does not converge to f locally uniformly. Now, $\{f_{n_{k_m}}\}_{m=1}^{\infty}$ is also a subsequence of the original sequence, which must converge locally uniformly to the same limit f with Beltrami coefficient μ. Hence, we obtain a contradiction. This implies the original sequence converges locally uniformly to f, whose Beltrami coefficient is equal to μ. □

With the above formulations, our proposed algorithm to extract the multi-scale representations of a deformation can be described as follows.

Algorithm 1: *Multi-scale representation of deformation*

Input: Images I_1 and I_2 capturing an object at $t = 0$ and $t = 1$.
Output: $\{I^{(j)}\}_{j\in\mathbb{Z}}$ = sequence of images capturing deformations of I_1 at various scales.

1 Compute the registration f between I_1 and I_2 as described in section 4.1;
2 Compute the Beltrami coefficient $\mu(f)$ of f using equation (4.2);
3 Compute the wavelet expansion of $\mu(f)$ to obtain $\hat{\mu}(i, j, k_1, k_2)$ for $1 \leq i \leq 3$, $j, k_1, k_2 \in \mathbb{Z}$;
4 For each $j \in \mathbb{Z}$, compute $\mathcal{P}_j(\mu(f))$ and $f_j := \mathbf{LBS}(\mathcal{P}_j(\mu(f)))$;
5 For each $j \in \mathbb{Z}$, compute $I^{(j)} := I_1 \circ f_j^{-1}$;

Remark: Algorithm 1 decomposes a deformation into components of different scales over the entire domain. Sometimes, it is required to decompose a deformation into components of various scales over a particular region Ω. In this case, $\widetilde{\mu}(\Omega, j)$ should be computed and $f_j := \mathbf{LBS}(\mathcal{P}_j(\mu(f)))$ in step 4 should be replaced by $f_j^{\Omega} := \mathbf{LBS}(\widetilde{\mu}(\Omega, j))$.

5. Experimental Result. We have tested our proposed algorithm on synthetic examples together with real data. There are different choices of mother wavelet to be used in our model, such as Haar, spline, Daubechies, biorthonal wavelets and so on. In this work, we choose the biorthogonal wavelet 6.8 in Matlab for our deformation extraction. Experimental results are reported in this section.

5.1. Synthetic examples.
Example 1:. In this synthetic example, a circular object is being deformed to a star-shaped object. The unit circle and the deformed star-shaped boundaries are shown in Figure 5.1(a) and (b) respectively, which are labeled in red as landmarks.

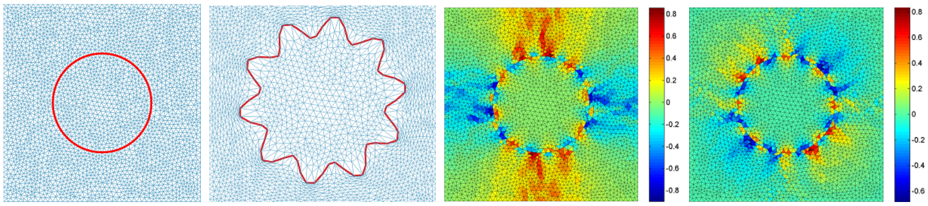

(a) Original mesh (b) Deformed mesh (c) Re(μ) (d) Imag(μ)

Fig. 5.1: Example 1: Deformation from a circle to a star-shaped contour. The unit circle and the deformed star-shaped contour are shown in (a) and (b) respectively. (c) and (d) show the real and imaginary part of BC corresponds to the deformation respectively.

The landmark-based registration between the two images and its associated Beltrami coefficient are computed. The real and imaginary parts of the BC are shown in (c) and (d) respectively. The wavelet coefficients of the BC can be computed. The wavelet expansion approximates the input BC. Figure 5.2(a) and (b) shows the real and imaginary parts of the reconstructed BC from the full set of wavelet coefficients. They closely resemble to the original BC. The local and global components of the deformation can be extracted by removing the low and high frequency components in the wavelet expansion respectively. The extracted local deformation is shown in (c). It deforms the original circle to a star-shaped contour of similar size. The extracted global deformation is shown in (d). It deforms a unit circle to a bigger circle. This demonstrates that the original deformation consists of two main components, namely, 1. a deformation from a circle to a star-shaped contour and 2. a global scaling. (e) shows the spectrum of the wavelet coefficients. The upper left corner corresponds to the wavelet decomposition coefficients at the global scale, while the coefficients in the lower layers represent the wavelet decomposition coefficients at the local scale.

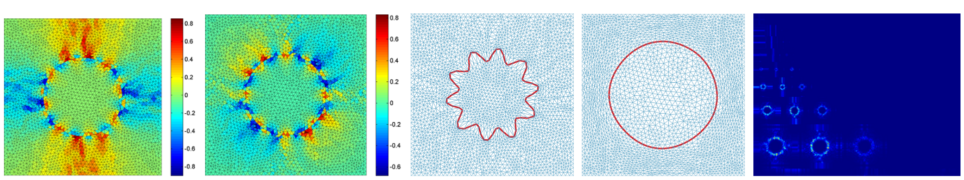

(a) (b) (c) (d) (e)

Fig. 5.2: Example 1: Multi-scale representation of the deformation from a circle to a star-shaped contour. (a) and (b) show the reconstruction of the real and imaginary part of BC respectively using the full set of coefficients. (c) and (d) show the extracted local and global deformation respectively. (e) shows the spectrum of the wavelet decomposition coefficients.

Example 2:. In this example, we compute the multi-scale representation of a deformation consisting of deformations at three different scales. The boundary of the

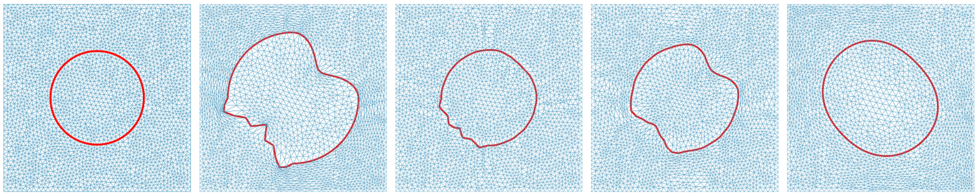

(a) Original (b) Registered (c) Local (d) Intermediate (e) Global

Fig. 5.3: (a) and (b) show the original mesh and the registration result of Example 2, where the landmarks are marked in red. (c), (d) and (e) shows the deformation components at the local, intermediate and global scales respectively.

original object is a circle as shown in Figure 5.3(a), which is deformed to another shape as shown in Figure 5.3(b). Using our proposed algorithm, we successfully extract the three deformation components at different scales. (c), (d) and (e) shows the deformation components at the local, intermediate and global scales respectively.

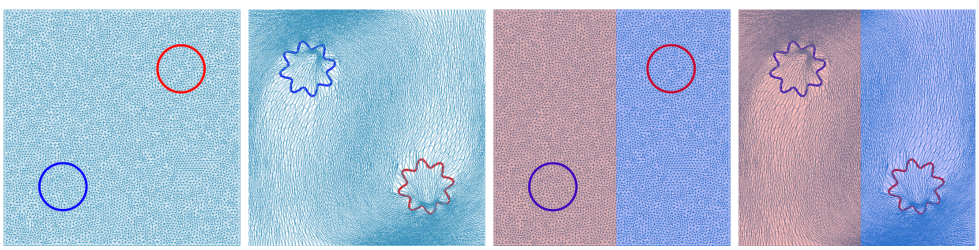

(a) Original (b) Registered (c) Mask on (a) (d) Mask on (b)

Fig. 5.4: (a) and (b) show the original mesh and the registration result of Example 3, where the landmarks are marked in red and blue. (c) and (d) show the mask for the wavelet decomposition coefficients for extracting multi-scale deformation components at different locations.

Example 3:. In this example, we consider a deformation consisting of a large global deformation and a local deformation. Figure 5.4(a) shows the boundaries of the initial objects, which are marked in blue and red colors. The blue object is moved upward and the red object is moved downward. Both objects are deformed locally to star-shaped contours. We proceed to obtain the deformation components at different scales and different locations. (c) and (d) show the mask for the wavelet decomposition coefficients for extracting multi-scale deformation components. Figure 5.5(a) shows the spectrum of the wavelet decomposition coefficients. The red and blue region represent the mask for choosing the wavelet coefficients to obtain the deformation components at different locations. (b) shows the global deformation component. (c) shows the extracted local deformation component of the blue object. (d) shows the local deformation component of the red object. Note that the local and global deformation components at different locations are successfully extracted. Figure 5.6(a) and (b) show the extraction of the deformation component using the

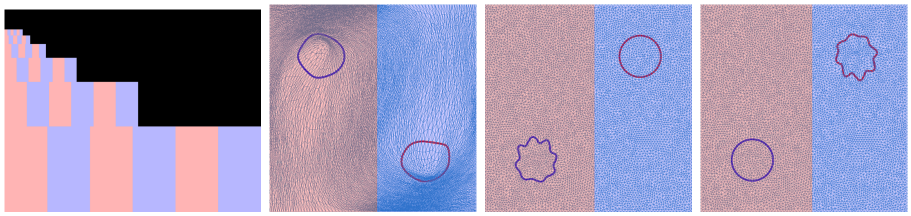

(a) Spectrum (b) Global (c) First local (d) Second local

Fig. 5.5: (a) shows the spectrum of the wavelet decomposition coefficients. The red and blue region represent the mask for choosing the wavelet decomposition coefficients at different locations. (b), (c) and (d) shows the global, first and second local deformation components.

wavelet transformation directly applied on the Euclidean coordinates of the mapping. Note that abnormal squeezing and overlaps appear.

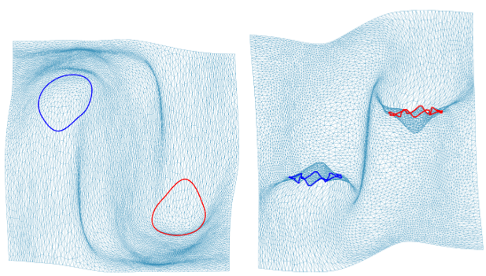

(a) (b)

Fig. 5.6: (a) and (b) show the extraction of the deformation in Example 3 using wavelet transform directly applied on the Euclidean coordinates of the mapping. Note that abnormal squeezing and overlaps appear.

Example 4:. Figure 5.7(a) and (b) shows the original and deformed objects. We proceed to extract the local and global deformation components at different scales and locations. (c) and (d) shows the mask for extracting the local deformation components at different locations. The spectrum of the wavelet coefficients are shown in (e). The different regions represent the masks for choosing the wavelet decomposition coefficients at different locations. Figure 5.8(a) shows the extracted global deformation component. (b), (c), (d) and (e) shows the local deformation components at the bottom-left, bottom-right, top-right and top-left respectively.

5.2. Real examples.

Example 5: Spine. In this example, we test our proposed algorithm for the multiscale deformation decomposition on real spine images. Figure 5.9(a) shows a spine image of a young age control subject. (b) shows a spine image of a grown-up patient. Our goal is to extract the global and local components of the deformation

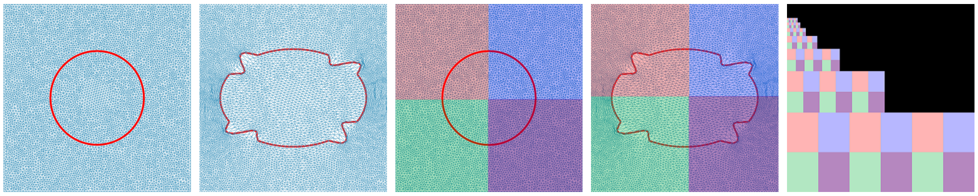

(a) Original (b) Deformed (c) Mask on (a) (d) Mask on (b) (e) Spectrum

Fig. 5.7: (a) and (b) show the original and deformed mesh of Example 4. (c) and (d) show the mask for extracting the decomposition coefficients at different locations of Example 4, which are divided by the red, blue, green and purple region respectively. (e) shows the spectrum of the wavelet decomposition coefficients of Example 4.

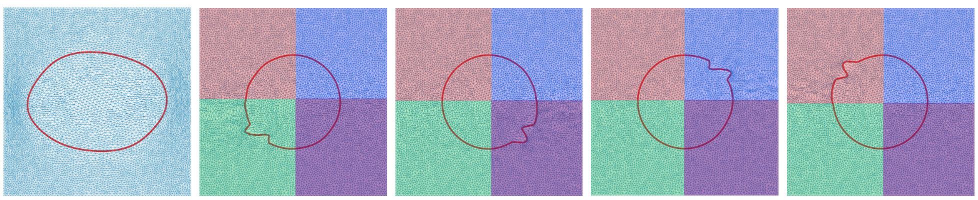

(a) Global (b) First local (c) Second local (d) Third local (e) Fourth local

Fig. 5.8: (a) shows the extracted global deformation component of Example 4. (b), (c), (d) and (e) shows the local deformation components at the bottom-left, bottom-right, top-right and top-left regions respectively.

of the spine. A triangular mesh is built on the images and corresponding feature landmarks to drive the registration, are shown in Figure 5.9(c) and (d). The extracted global and local deformations from the control spine are shown in Figure 5.9(e) and (f) respectively. The meshes show how to global and local diffeomorphism deforms the image. (g) and (h) show the deformed spine images without meshes by the global and local deformation respectively. Our proposed model successfully decomposes the deformation into global and local components.

Example 6: Corpus callosum. In this example, we apply our proposed model on corpus callosum images. Figure 5.10(a) shows the image of a healthy corpus callosum. (b) shows the image of the corpus callosum of a patient suffering from progressive supranuclear palsy (PSP). Triangular meshes are built on each images and corresponding feature landmarks are labeled to drive the registration, which are shown in (c) and (d). Figure 5.10(e) and (f) shows how the mesh of the image from the healthy subject is deformed under the extracted global and local deformations respectively. (g) and (h) shows the deformed images by the global and local deformations. Our model successfully decomposes the deformation into global and local components.

Figure 5.11(a) and (b) show the corpus callosum images of a healthy subject and a patient suffering from normal pressure hydrocephalus (NPH) respectively. Meshes are built on each images and corresponding feature landmarks are labeled (See (c)

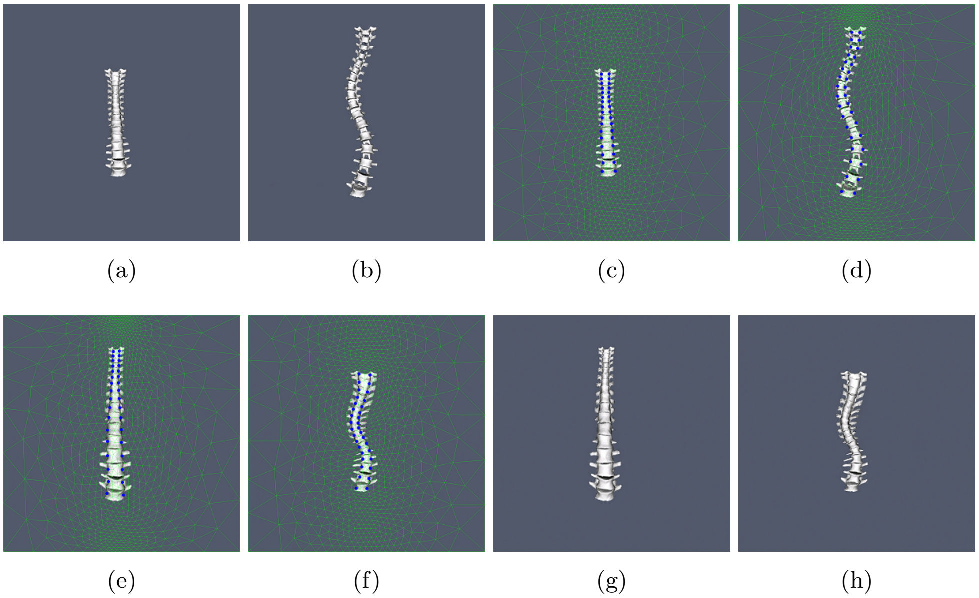

Fig. 5.9: (a) shows the original spine image. (b) shows the deformed spine image of a grown-up patient. (c) and (d) show the landmark points in (a) and (b) marked in blue respectively. A triangular mesh is built on the images. (e) and (f) show the global and local components of the spine deformation by using our proposed algorithm. (g) and (h) show the corresponding deformed images.

and (d)). Figure 5.10(e) and (f) show how the mesh of the image from the healthy subject is deformed under the extracted global and local deformations respectively. (g) and (h) shows the deformed image by the global and local deformations. Again, our model successfully decomposes the deformation into global and local components.

6. Conclusion. In this work, we propose a novel algorithm for the multiscale decomposition of deformations via quasi-conformal theories. Our work focuses on the decomposition of deformations at different geometric scales and locations. A deformation is described as a diffeomorphism. Given a diffeomorphism f, we first represent the diffeomorphism using the Beltrami coefficient (BC), which is a complex-valued function measuring the conformality distortion of the diffeomorphism. With this representation, we propose to apply the wavelet transformation on the BC to decompose it into various components of different frequencies compactly supported at different sub-domains. Quasi-conformal map associated to different components of the BC can be reconstructed by solving the Beltrami's equation. The multiscale decomposition of the deformation can then be constructed. To validate our proposed algorithm, we have applied it on synthetic examples as well as real medical data. Results demonstrate our model can successfully decompose the deformation at multiple geometric scales and locations.

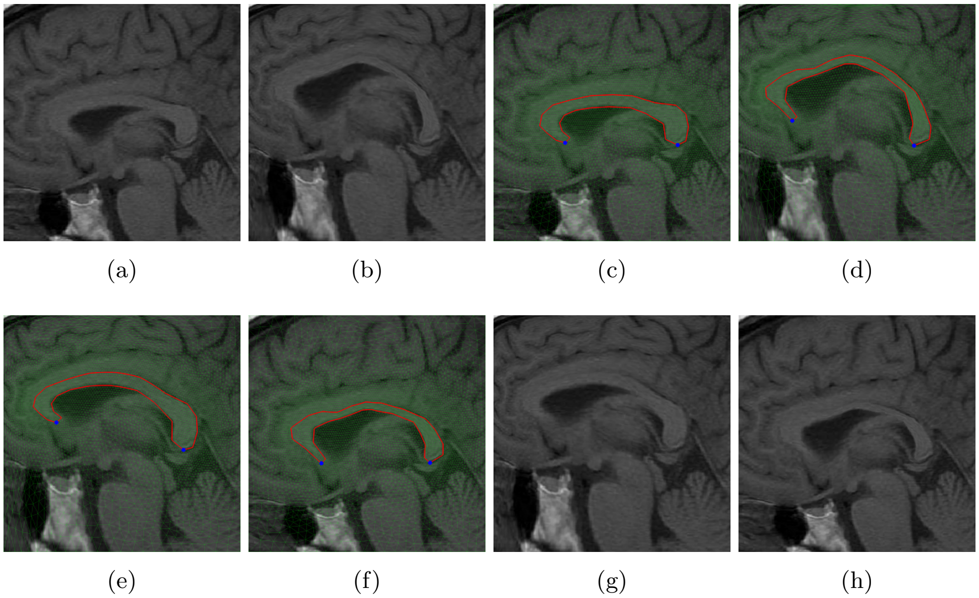

Fig. 5.10: (a) shows the image of a healthy corpus callosum. (b) shows the image of the corpus callosum of a patient suffering from progressive supranuclear palsy (PSP). (c) and (d) show the feature landmarks (blue and red) which extract the corpus callosum in (a) and (b) respectively. Triangular meshes are built on each images for registration. (e) and (f) show how the mesh of the image from the healthy subject is deformed under the extracted global and local deformations respectively. The deformed images by the global and local deformations are shown in (g) and (h) respectively.

Acknowledgment. Lok Ming Lui is supported by RGC GRF (Project ID: 401811).

REFERENCES

[1] M. K. Abeyratne, W. Freeden, and C. Mayer. Multiscale deformation analysis by cauchy-navier wavelets. *Journal of Applied Mathematics*, 12:605–645, 2003.
[2] D. Bechmann. Space deformation models survey. *Computers & Graphics*, 18(4):571–586, 1994.
[3] B. Bijnens, P. Claus, F. Weidemann, J. Strotmann, and G. R. Sutherland. Investigating cardiac function using motion and deformation analysis in the setting of coronary artery disease. *Circulation*, 116(21):2453–2464, 2007.
[4] F. L. Bookstein. Principal warps: Thin-plate splines and the decomposition of deformations. *IEEE Transactions on Pattern Analysis and Machine Intelligence*, 11(6):567–585, 1989.
[5] G. Chen, K. Mischaikow, R. S. Laramee, and E. Zhang. Efficient morse decompositions of vector fields. *IEEE Transactions on Visualization and Computer Graphics*, 4(14):848–862, 2008.
[6] Lam K. C. Choi, P. T. and L. M.: Lui. Lash: Fast landmark aligned spherical harmonic parameterization for genus-0 closed brain surfaces. *SIAM Journal on Imaging Sciences*, 8(1):67–94, 2015.
[7] A. Fletcher and V. Markovic. *Quasiconformal maps and Teichmüller theory*. Oxford graduate texts in mathematics. Oxford University Press, Oxford, 2007.
[8] F. P. Gardiner and N. Lakic. *Quasiconformal Teichmüller theory*. Mathematical surveys and monographs. American Mathematical Society, 2000.
[9] B. Glocker, N. Komodakis, G. Paragios, N.and Tziritas, and N. Navab. Inter and intra-modal

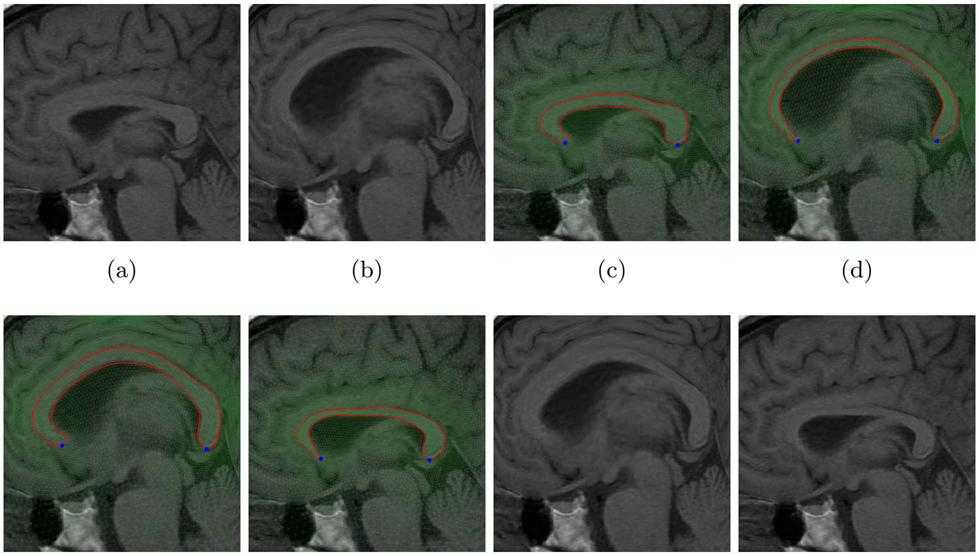

(a) (b) (c) (d)

(e) (f) (g) (h)

Fig. 5.11: (a) shows the image of a healthy corpus callosum. (b) shows the image of the corpus callosum of a patient suffering from Normal Pressure Hydrocephalus (NPH). (c) and (d) show the feature landmarks (blue and red), which extract the corpus callosum in (a) and (b) respectively. Triangular meshes are built on each images for registration. (e) and (f) show how the meshes of the image from the healthy subject is deformed under the extracted global and local deformations respectively. The deformed images by the global and local deformations are shown in (g) and (h) respectively.

deformable registration: Continuous deformations meet efficient optimal linear programming. *Information Processing in Medical Imaging. Springer Berlin Heidelberg*, pages 408–420, 2007.

[10] B. Glocker, A. Sotiras, N. Komodakis, and N. Paragios. Deformable medical image registration: Setting the state of the art with discrete methods. *Annual review of biomedical engineering*, 13:219–244, 2011.

[11] P. Golland, W. E. L. Grimson, M. E. Shenton, and R. Kikinis. Deformation analysis for shape based classification. *Information Processing in Medical Imaging*, pages 517–530, 2001.

[12] P. Golland, W. E. L. Grimson, M. E. Shenton, and R. Kikinis. Detection and analysis of statistical differences in anatomical shape. *Medical image analysis*, 9(1):69–86, 2005.

[13] P. S. Heckbert. Survey of texture mapping. *Computer Graphics and Applications, IEEE*, 6(11):56–67, 1986.

[14] J. R. Kaplan and D. L. Donoho. The morphlet transform: A multiscale representation for diffeomorphisms. *DEFORM06-Proceedings of the Workshop on Image Registration in Deformable Environments*, 12:21–, 2003.

[15] D. Kihara, L. Sael, R. Chikhi, and J. Esquivel-Rodriguez. Molecular surface representation using 3D Zernike descriptors for protein shape comparison and docking. *Current Protein and Peptide Science*, 12(6):520–530, 2011.

[16] K.C. Lam and L.M. Lui. Landmark and intensity based registration with large deformations via quasi-conformal maps. *SIAM Journal on Imaging Sciences*, 7(4):2364–2392, 2014.

[17] O. Lehto and K. I. Virtanen. *Quasiconformal mappings in the plane*. Die Grundlehren der mathematischen Wissenschaften in Einzeldarstellungen mit besonderer Berücksichtigung der Anwendungsgebiete. Springer, Berlin, Heidelberg, New York,, 2nd edition, 1973.

[18] L. M. Lui, K. C. Lam, T. W. Wong, and X. F. Gu. Texture map and video compression using Beltrami representation. *Siam Journal on Imaging Sciences*, 6(4):1880–1902, 2013.

[19] L. M. Lui, Y. L. Wang, T. F. Chan, and P. Thompson. Landmark constrained genus zero surface conformal mapping and its application to brain mapping research. *Applied Numerical Mathematics*, 57(5-7):847–858, 2007.

[20] L. M. Lui, T. W. Wong, Gu X. Zeng, W., P. M. Thompson, T. F. Chan, and S. T. Yau. Detection of shape deformities using Yamabe flow and Beltrami coefficients. *Inverse Problems and Imaging*, 4(2):311–333, 2010.

[21] L. Peng, Z. Y. Huang, and Y. Y. Jia. Application of the combinatorial model of wavelet analysis and support vector machines in deformation analysis. *Remote Sensing, Environment and Transportation Engineering (RSETE)*, pages 1–4, 2012.

[22] P. Rgen and H. Bohr. A new family of global protein shape descriptors. *Mathematical biosciences*, 182(2):167–181, 2003.

[23] A. M. Shah and S. D. Solomon. Myocardial deformation imaging current status and future directions. *Circulation*, 152(2):244–248, 2012.

[24] S. Sommer, M. Nielsen, F. Lauze, and X. Pennec. A multi-scale kernel bundle for LDDMM: towards sparse deformation description across space and scales. *Information Processing in Medical Imaging, Springer Berlin Heidelberg*, pages 624–635, 2011.

[25] A. Sotiras, C. Davatzikos, and N. Paragios. Deformable medical image registration: A survey. *IEEE Transactions on Medical Imaging*, 32(7):1153–1190, 2013.

[26] V. Taimouri and J. Hua. Deformation similarity measurement in quasi-conformal shape space. *Graphical Models*, 76(2):57–69, 2014.

[27] J. P. Thirion. Image matching as a diffusion process: an analogy with Maxwell's demons. *Medical Image Analysis*, 2(3):243–260, 1998.

[28] Y. Tong, S. Lombeyda, A. N. Hirani, and M. Desbrun. Discrete multiscale vector field decomposition. *ACM Transactions on Graphics (TOG)*, 22(3):445–452, 2003.

[29] T. Vercauteren, X. Pennec, A. Perchant, and N. Ayache. Diffeomorphic demons: Efficient non-parametric image registration. *Neuroimage*, 45(1):S61–S72, 2009.

[30] D. F. Walnut. *An introduction to wavelet analysis*. Applied and Numerical Harmonic Analysis. Springer Science & Business Media., New York, USA, 2013.

[31] H. Wang and A. Amini. Cardiac motion and deformation recovery from MRI: a review. *Medical Imaging, IEEE Transactions on*, 31(2):487–503, 2012.

[32] G. Welch and E. Foxlin. Motion tracking survey. *IEEE Computer graphics and Applications*, pages 24–38, 2002.

[33] D. Zhang and G. Lu. Review of shape representation and description techniques. *Pattern recognition*, 37(1):1–19, 2004.

[34] B. Zitova and J. Flusser. Image registration methods: a survey. *Image and Vision Computing*, 21(11):977–1000, 2003.